ACS APPLIED MATERIALS & INTERFACES

www.acsami.org

Forum Article

In Situ Liquid Phase TEM of Nanoparticle Formation and Diffusion in a Phase-Separated Medium

Youngju Son,[†] Byung Hyo Kim,[†] Back Kyu Choi,[†] Zhen Luo, Joodeok Kim, Ga-Hyun Kim, So-Jung Park, Taeghwan Hyeon,* Shafigh Mehraeen,* and Jungwon Park*

Cite This: https://doi.org/10.1021/acsami.1c20824

Read Online

ACCESS | Metrics & More | Article Recommendations | Supporting Information

ABSTRACT: Colloidal nanoparticles are synthesized in a complex reaction mixture that has an inhomogeneous chemical environment induced by local phase separation of the medium. Nanoparticle syntheses based on micelles, emulsions, flow of different fluids, injection of ionic precursors in organic solvents, and mixing the metal organic phase of precursors with an aqueous phase of reducing agents are well established. However, the formation mechanism of nanoparticles in the phase-separated medium is not well understood because of the complexity originating from the presence of phase boundaries as well as nonuniform chemical species, concentrations, and viscosity in different phases. Herein, we investigate the formation mechanism and diffusion of silver nanoparticles in a phase-separated medium by using liquid phase transmission electron microscopy and many-body dissipative particle dynamics simulations. A quantitative analysis of the individual growth trajectories reveals that a large portion of silver nanoparticles nucleate and grow rapidly at the phase boundaries, where metal ion precursors and reducing agents from the two separated phases react to form monomers. The results suggest that the motion of the silver nanoparticles at the interfaces is highly affected by the interaction with polymers and exhibits superdiffusive dynamics because of the polymer relaxation.

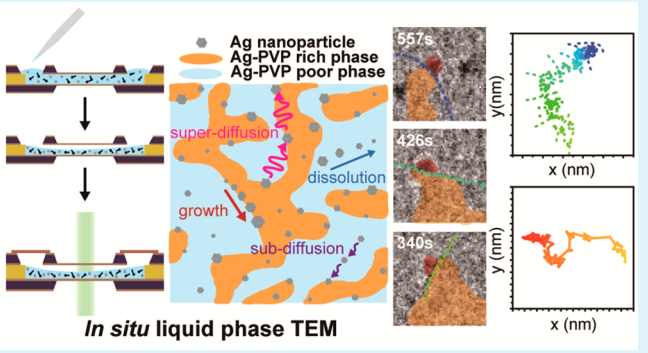

KEYWORDS: *colloidal nanoparticle, phase separation, liquid phase TEM, interface, diffusion*

Downloaded via SEOUL NATL UNIV on March 15, 2022 at 07:42:05 (UTC).
See https://pubs.acs.org/sharingguidelines for options on how to legitimately share published articles.

INTRODUCTION

Many chemical reactions incorporate multiple phases in a reaction medium. These reactions dynamically interact with each other. Examples include chemical transduction across a cellular matrix,[1,2] synthesis of polymers,[3] colloid formation,[4,5] and phase-transfer catalytic synthesis of organic molecules.[6] Colloidal nanoparticles are also synthesized by exploiting inhomogeneous chemical environment generated by a phase-separated medium. Metal nanoparticles smaller than 5 nm in diameter are conventionally synthesized from the reaction mixture composed of an organic phase containing metal precursors and an aqueous phase with reducing agents.[7,8] In addition, fine control of the nanoparticle synthesis with respect to the size, the crystal structure, and the morphology has been achieved in methods based on micelles,[9,10] emulsions,[11,12] flow of different fluids,[13,14] and injection of ionic precursors in organic solvents.[15]

Despite the experimental success of the nanoparticle synthesis in these systems, the formation mechanism of nanoparticles in the phase-separated medium is not well understood because of the complexity originating from the presence of phase boundaries as well as nonuniform chemical species, concentrations, and viscosity of different phases.[16,17] In addition, the dimension of the phase-separated domains in the nanoparticle synthesis can be small, in the range of nanoscale, and the phase boundary in the reaction mixture is presumably not static, and rather, continuously fluctuating.[18−20] The liquid phase transmission electron microscopy (LPTEM) has the capability to directly visualize chemical reactions in a fluidic medium, possibly ideal for investigating the complex formation mechanism of nanoparticles in the phase-separated medium.[21−28] For example, it was found that there is spinodal decomposition occurring prior to nucleation in the formation of metal nanoparticles and metal-organic frameworks by using LPTEM.[29,30] LPTEM also revealed the structure of polymer vesicles in the assembly of a block copolymer.[31]

In this report, by using LPTEM and many-body dissipative particle dynamics (MDPD) simulations, we investigate the formation and diffusion of silver nanoparticles in a complex

Special Issue: Early Career Forum

Received: October 28, 2021
Accepted: January 21, 2022

© XXXX American Chemical Society

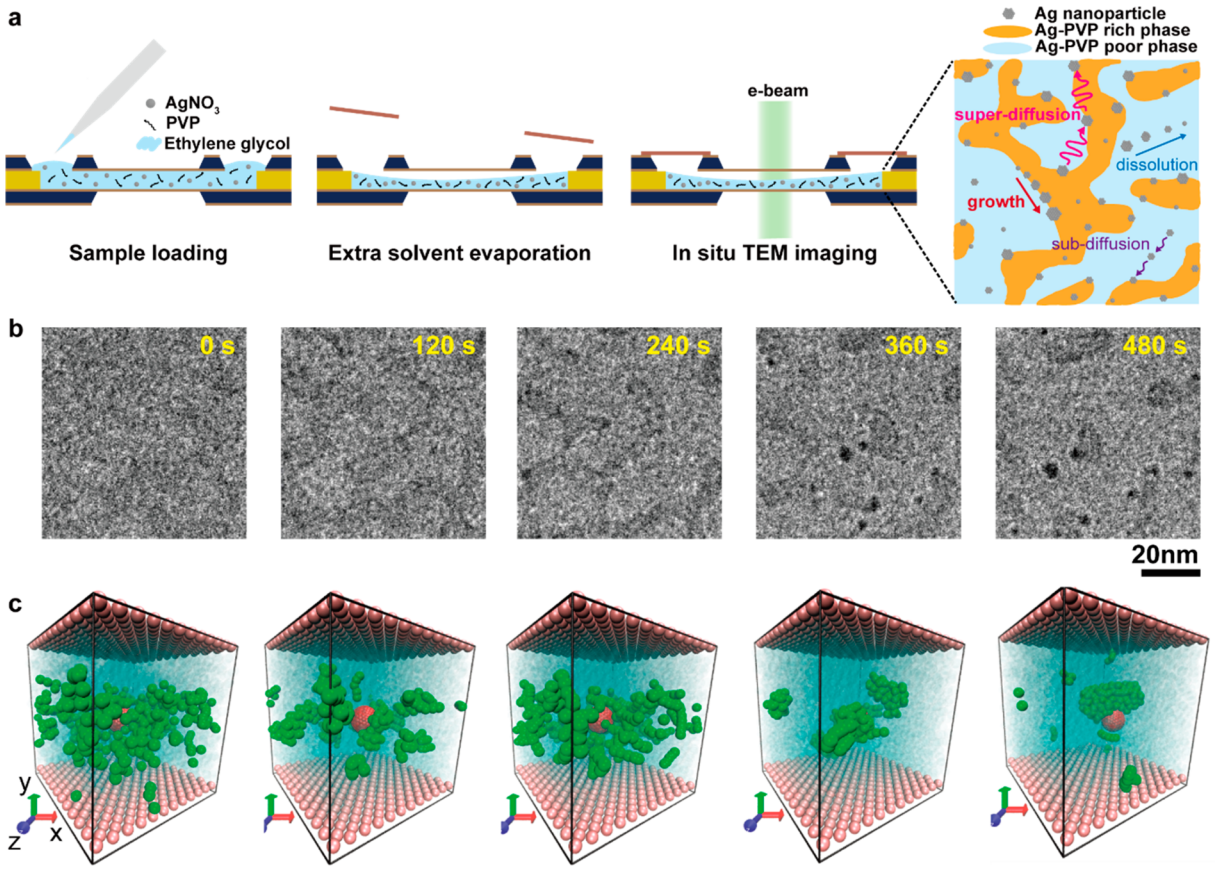

Figure 1. Formation of a phase-separated medium and nanoparticles in the LPTEM. (a) Left to right, schematics of LPTEM experiments including (i) loading the solution containing poly(vinylpyrrolidone) (PVP) polymers and metal precursors, (ii) evaporating the solvent, and (iii) sealing the liquid cell and imaging the samples in TEM. In the liquid cell, polymer solution is separated into a Ag-PVP-rich phase and a Ag-PVP-poor phase. A large portion of nanoparticles nucleate, grow rapidly, and exhibit superdiffusive dynamics. (b) Snapshots of a TEM movie that show the phase-separated medium and growth of nanoparticles at t = 0, 120, 240, 360, and 480 s. (c) Left to right, snapshots from MDPD simulations at t = 0.1, 1, 10, 100, and 1000 MDPD time units, respectively, illustrating the formation of a polymer-rich region (green beads), whereas the nanoparticle (red) resides at the interface of polymer-poor (cyan semitransparent beads) and -rich phases. Pink beads indicate the top and bottom plates, which encapsulate the polymer-poor and -rich phases, in the LPTEM.

medium composed of two phases with different concentrations of polymer ligand molecules and metal ion precursors. The LPTEM observations reveal that the interface of the two phases plays a critical role in the synthesis of nanoparticles and drives the motion of synthesized nanoparticles.

EXPERIMENTAL SECTION

Materials. Silver nitrate ($AgNO_3$, 99.9%), ethylene glycol (99%), and poly(vinylpyrrolidone) (PVP, M_w = 40 000) were purchased from Sigma-Aldrich and used without further purification. Silicon (100 μm)/silicon nitride (50 nm) wafers were purchased from Semirod. Photoresist (AZ-5214 and MIF-715) solutions were purchased from MicroChemicals. Potassium hydroxide solution was purchased from Samchun Chem.

Liquid Phase TEM Experiment. We prepared top and bottom chips of liquid cells for TEM via photolithography. For this experiment, 50 nm silicon nitride thin films were deposited onto the 100 μm thick silicon wafers using the chemical vapor deposition method. Rectangular-shaped windows were patterned on the wafers using photolithography for each grid. Silicon nitride was selectively etched with SF_6 gas in a reactive ion etcher, and silicon was etched with potassium hydroxide solution. Indium spacers were deposited to a thickness of 20 nm using a thermal evaporator. A schematic illustration of the fabrication processes is depicted in Figure S1a.

The top and bottom chips were aligned and bonded via indium spacers. We prepared a 0.01 M $AgNO_3$/poly(vinylpyrrolidone) (PVP) ethylene glycol solution. The precursor–polymer solution was loaded into the reservoir of the liquid cell. The liquid cell was sealed with a vacuum grease-applied aperture grid with a hole size of 600 μm (Figure S1b). The entire manufacturing process was inspected to check for breakage of windows, the alignment of the two chips, and contamination (Figure S2).

The solution in the liquid cells was imaged with TEM with an acceleration voltage of 200 kV and beam current of <5000 e/A^2. The resulting in situ TEM images were processed using homemade *MATLAB* code that binarized the TEM images into black and white images. The code utilizes the Gaussian, Wiener, and Laplacian filters and the Bradley–Roth method. We tracked translational motion of individual nanoparticles, as shown in Figure S3.

RESULTS AND DISCUSSION

The formation of silver nanoparticles from ethylene glycol solution containing PVP and $AgNO_3$ in a silicon nitride liquid cell is monitored by LPTEM (Figure 1a). Evaporating the extra ethylene glycol solvent in a liquid cell before TEM imaging promotes a condition that readily induces a spinodal decomposition of the solution, two phases of which have high and low concentration of PVP and $AgNO_3$ (Ag-PVP-rich and Ag-PVP-poor phases, respectively). The in situ LPTEM image series clearly shows the formation of the two phases, exhibiting different contrast (Figure 1b, Figure S4, and Figure S5). The

https://doi.org/10.1021/acsami.1c20824
ACS Appl. Mater. Interfaces XXXX, XXX, XXX–XXX

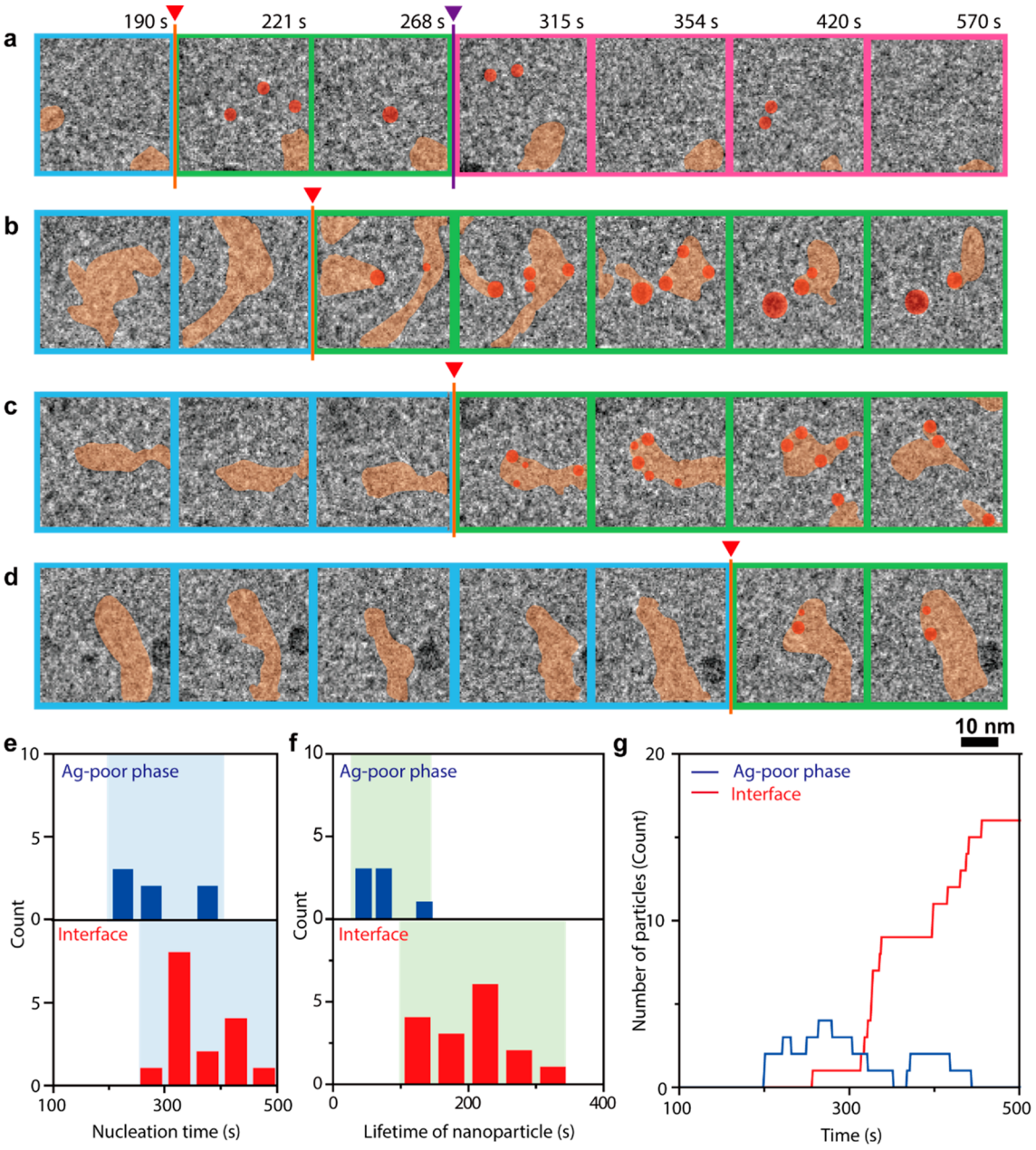

Figure 2. Inhomogeneity in the nucleation and growth of nanoparticles in the phase-separated medium. Snapshots of nanoparticles (at t = 190, 221, 268, 315, 354, 420, and 570 s) (a) in the Ag-PVP-poor phase and (b−d) at the interfaces. Blue-colored images represent the TEM images before nucleation and the green-colored ones show the TEM images of nanoparticles after nucleation. Red lines represent the nucleation time of nanoparticles. The pink-colored images indicate the TEM images after dissolution of nanoparticles. Purple line represents the dissolution time of nanoparticles. (e) Numbers of nucleation events in the Ag-PVP-poor phase (top) and at the interface (bottom). (f) Histogram of the lifetime of nanoparticles in the Ag-PVP-poor phase (top) and at the interface (bottom). (g) Temporal change in number of nanoparticles during a reaction for particles at the interface (red line) and those in the Ag-PVP-poor phase (blue line).

significant difference in solubility parameters of PVP and ethylene glycol, about 10 (Hildebrand value),[32,33] leads to a phase separation of the Ag-PVP-rich and Ag-PVP-poor phases. The different contrast is presumably from the different amount of Ag ions, having high electron density (Z = 47), dissolved in each phase. Because the Ag ions can interact with partially negatively charged carbonyl groups in PVP, more Ag ions are located in the Ag-PVP-rich phase, showing relatively darker in contrast.[34−36]

The phase separation is also supported by MDPD computer simulations.[37−39] MDPD is a coarse-grained particle-based computational method and can simulate multiphase mixtures on the mesoscale while accounting for hydrodynamic interactions.[40,41] Figure 1c illustrates the progression of polymer-poor (semitransparent cyan region) and -rich (green beads) phase separation at different times using MDPD simulations with k_b = 5. Here, k_b is the bending stiffness of the polymers normalized by kT in the simulations. To exclude the effect of the bottom and top plates in LPTEM on the dynamics of polymers and nanoparticles and their interactions with interface of the two phases, we prevented the polymers and nanoparticles from getting too close to the bottom and top plates by having a short-range repulsion between the plates and polymers and nanoparticles in the simulations. This way, the

https://doi.org/10.1021/acsami.1c20824
ACS Appl. Mater. Interfaces XXXX, XXX, XXX−XXX

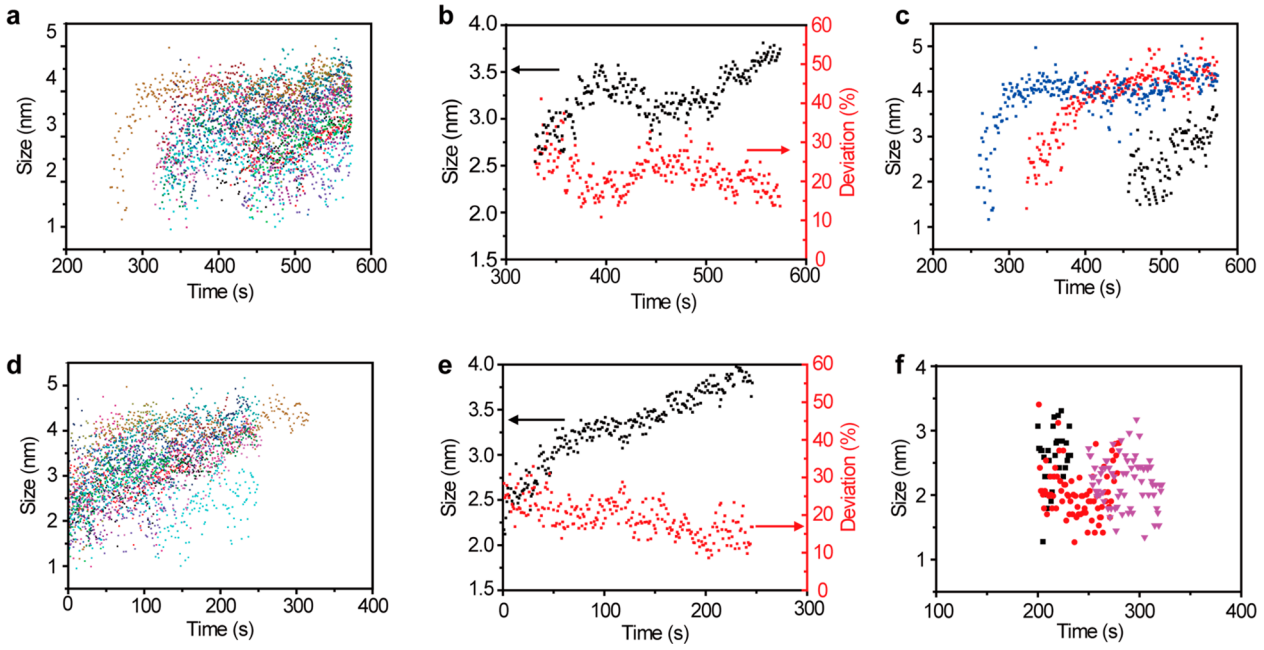

Figure 3. Growth of nanoparticles in the phase-separated medium. (a) Temporal size change of growing nanoparticles located at the interface. The number of growth trajectories is 17. (b) Average (black) and normalized standard deviation (red) of nanoparticle size at the interface. (c) Three representative growth trajectories selected from the 17 trajectories in panel a for comparison. The three trajectories have different nucleation times but show similar trends. (d) Individual growth trajectory of nanoparticles at the interface by setting $t_0 = 0$ for their nucleation to eliminate the effect of different nucleation time. (e) Average size and normalized standard deviation of nanoparticles at the interface after setting $t_0 = 0$ for their nucleation time. (f) Temporal variation in nanoparticle size in Ag-PVP-poor phase, showing a fast dissolution of the nanoparticles.

polymer-rich domain mostly stays in the bulk, as it will be energetically costly near either plate, so we can study only the interaction of the interface, polymers, and nanoparticles. The first panel in Figure 1c, which nearly represents the initial configuration of the polymer-poor and -rich domains, shows a random distribution of polymers (green beads) in the middle portion of the simulation box. As the polymers relax, and the system goes through the spinodal decomposition, the polymers aggregate, and the polymer-rich phase appears (green globular region in the far right panel in Figure 1c). During the simulations, the nanoparticle, shown in red (Figure 1c), stays almost at the interface of the polymer-poor and -rich phase. We summarize all parameters used in the simulations in Table S1.

Different chemical potentials of each phase and interface cause the inhomogeneity in the formation of Ag nanoparticles. We quantitatively analyze the formation of Ag nanoparticles in the two phases after the spinodal decomposition based on in situ LPTEM observations. Ag nanoparticles begin to nucleate after an induction period of about 200 s (Figure 1b, Figure S5). While ~30% of nanoparticles are nucleated in the Ag-PVP-poor phase, ~70% of them are generated within the Ag-PVP-rich phase along the interface between the two phases (Figure 1b, Figure 2a–d, and Figure S6). Interestingly, no noticeable nucleation events are observed in the middle of Ag-PVP-rich phase even if the concentration of Ag ions is supposedly high in this phase. The inhomogeneous distribution of nanoparticle formation indicates that the kinetics of nucleation events is highly influenced by the local chemical environment. The high frequency of nucleation at the interface between the two phases implies that encounter of Ag ions from Ag-PVP-rich phase and ethylene glycol from Ag-PVP-poor phase is important to initiate reductive nucleation to form Ag nanoparticles. It is worth noting that ethylene glycol is a well-known reducing agent used in bulk synthesis.[34,42] The important role of ethylene glycol in reductive formation of Ag nanoparticles is further supported by the absence of nucleation in the Ag-PVP-rich phase, where ethylene glycol is relatively diluted because of the high concentration of PVP and Ag ions.[42] This site-dependent unevenness of nucleation events is different from the expectation from the classical nucleation model.

In addition, the temporal distribution of nucleation events is deviated from the classical formation mechanism, where the nucleation bursts up within a short period of time. Contrary to the one-phase reaction, the nucleation time differs significantly depending on the location within the two phases. Monomers in the Ag-PVP-poor phase are nucleated within the 200–270 s time period (Figure 2a, e), whereas nucleation events on the interface mainly occur during the 250–460 s time frame (Figure 2b–e). The average nucleation time in the Ag-PVP-poor phase (268 ± 68 s) is shorter than that at the interface (365 ± 57 s), because ethylene glycol serving as a reducing agent is enriched in the Ag-PVP-poor phase. In addition, nucleation events at the interface occurs intermittently for this time period (Figure 2b–e). The supply of Ag ions and ethylene glycol probably relies on their diffusion from the different phases, slowing down the reduction reaction for the formation of monomers. Furthermore, such a reaction would become inevitably inhomogeneous along the interface because the structure of the interface thermally fluctuates.[43]

These observations indicate important factors for the formation of nanoparticles in a nonuniform reaction medium, regardless of the different dimensions of the interface. In a one-phase reaction, the reaction starts with a uniform concentration of metal ions, reducing agents, and ligand molecules. Then the monomer concentration abruptly decreases below the super-saturation level after its consumption in the burst of a

https://doi.org/10.1021/acsami.1c20824
ACS Appl. Mater. Interfaces XXXX, XXX, XXX–XXX

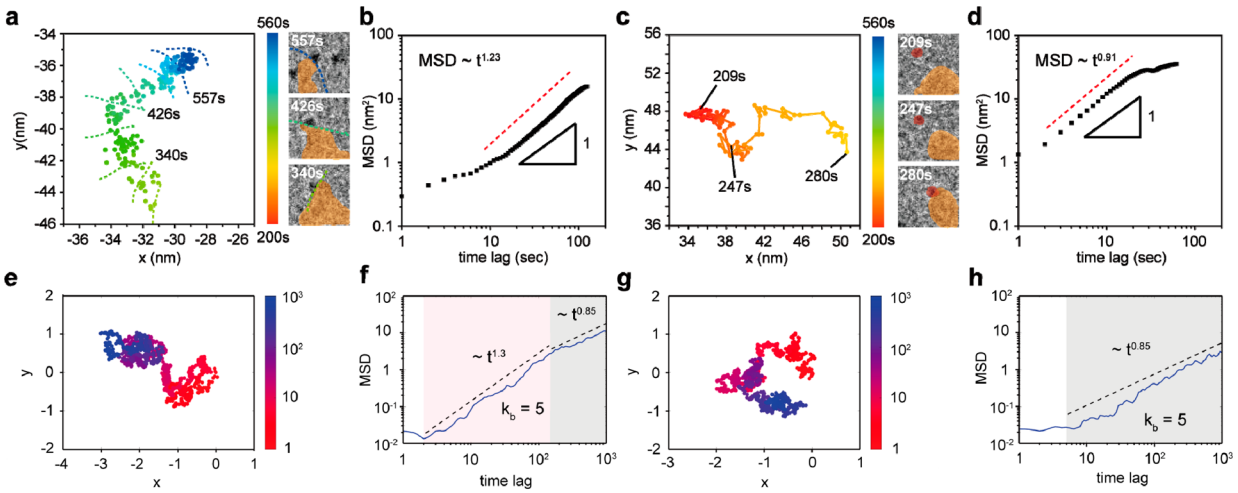

Figure 4. Diffusion of nanoparticles in the phase-separated medium. (a) Trajectory of a nanoparticle at the interface. Orange colored region represents the Ag-PVP-rich phase and the other region shows the Ag-PVP-poor phase. (b) MSD of nanoparticles at the interface taken from LPTEM images. MSD is proportional to $t^{1.23}$, indicating that the nanoparticle motion follows a superdiffusive dynamics. (c) A trajectory and (d) MSD of the nanoparticle in Ag-poor phase, showing subdiffusive dynamics. (e) Trajectory and (f) MSD of the nanoparticle at the interface taken from MDPD simulations. The bending stiffness of the polymer (k_b) is set to 5, nondimensionalized by kT. Gray and pink shaded areas represents the sub- and superdiffusive regime, respectively. (g) Trajectory and (h) MSD of the nanoparticle in the Ag-PVP-poor phase taken from MDPD simulations.

nucleation event, inhibiting further nucleation. After a nucleation, monomers are mainly used for the growth of the nanoparticles that are already nucleated. Unlike this, for systems that incorporate a nonuniform medium, it is suggested that the nucleation events can be site-dependent in different phases.[29] Furthermore, the interface plays an important role in proceeding the reaction that is highly diffusion controlled and kinetically inhomogeneous.

The growth processes in the two phases are also different because of the difference in monomer concentration and its variation, as well as the viscosity of the media in the two phases, which are correlated with the diffusion. Tracking individual growth trajectories of Ag nanoparticles in LPTEM enables classification of the trajectories corresponding to the nanoparticle locations, either at the interface or in the middle of the phases. The growth trajectories of nanoparticles in the Ag-poor phase have short lifetime of 69 ± 30 s on average (Figure 2f). Most of those nanoparticles dissolve, whereas some of them move and stick onto the interface (Figure 2a, f). As the desorption of monomers from nanoparticles becomes faster than the adsorption of monomers onto the nanoparticle surface in the Ag-PVP-poor phase with low monomer concentration, nanoparticle can be dissolved at a later time. In addition, the high interfacial energy at the two-phase interface is likely to induce anchoring of the survived diffusing Ag nanoparticles.

On the other hand, nanoparticles, which mainly stay in the Ag-PVP-rich side at the interface, mostly survive and grow for a prolonged period of time allowed in LPTEM. This is probably because the monomers are continuously supplied from the Ag-PVP-rich phase; hence, extend the growth of nanoparticles with the average lifetime of 207 ± 56 s (Figure 2f, g). MDPD simulations also confirm that, during the phase separation and formation of a polymer-rich phase, the nanoparticle persists at the interface of the two phases (Figure 1c). The average size of the nanoparticles at the interface does not monotonically increase but rather fluctuates, because nucleation events occur intermittently while the preformed nanoparticles are growing (Figure 3a, b). Such concurrence of the extended nucleation and growth events results in fluctuating average size of growing nanoparticles with large standard deviation. Nonetheless, from single particle growth trajectories, it is clear that nanoparticles grow in time (Figure 3c). Each nanoparticle grows rapidly for the initial 50 s right after its nucleation because of the abundant monomer concentration. After consumption of the surrounding monomers, the slow diffusion rate of monomers prevents them from being effectively supplied to the nanoparticles and thus decelerates the growth rate. If all trajectories are plotted from $t_0 = 0$ corresponding to the start of nucleation time (Figure 3d), all nanoparticles show similar trajectories, leading to a focused size distribution (Figure 3e). In contrast to the nanoparticles at the interface, the nanoparticles in the Ag-PVP-poor phase do not grow; rather, they dissolve out because of the low monomer concentration (Figure 3f).

It is expected that the growing nanoparticles have different diffusive motions depending on their locations in the phase-separated medium because of the locally different viscosities and concentrations of PVP polymers that interact with nanoparticles. It is noteworthy that PVP is known to strongly interact with the metallic surfaces, making it an efficient stabilizer for colloidal metallic nanoparticles.[34−36] Interestingly, the nanoparticles at the interface do not escape from the interface while their motion is synchronized with the fluctuation of the interface (Figure 4a and Figures S3 and S7a). The nanoparticle motion along the interface is characterized by analyzing the mean squared displacement (MSD) of the nanoparticle. The analysis shows that a significant portion of nanoparticles at the interface undergoes superdiffusive dynamics, which indicates that the nanoparticle motion is affected by an external motion (Figure 4b, Figure S8).[44,45] The driving force for the nanoparticles to follow superdiffusive dynamics and stay at the interface is the strong binding of the nanoparticles with PVP in Ag-PVP-rich phase (Figure S9).[34−36] Note that this observation is different from nanoparticle motions that show subdiffusive dynamics induced

https://doi.org/10.1021/acsami.1c20824
ACS Appl. Mater. Interfaces XXXX, XXX, XXX−XXX

by the interaction with silicon nitride membrane, reported in the previous LPTEM studies.[46−48] Because of the diffusion of the nanoparticles at the interface, they do not undergo coalescence or aggregation, which are commonly observed in the nanoparticle synthesis as a route to form polydispersity in nanoparticle size distribution. This implies that the interfacial synthesis of nanoparticles in a highly viscous medium can be utilized to improve their monodispersity. In contrast to the MSD of nanoparticles at the interfaces, the nanoparticles in the Ag-PVP-poor phase do not show a superdiffusive dynamics (Figure 4c, Figure S7b, and Figure S10). MSD analysis of the nanoparticles in the Ag-PVP-poor phase shows subdiffusive dynamics, indicating that nanoparticles in the Ag-PVP-poor phase are not influenced by external motions or forces (Figure 4d).[44,45] However, once freely moving nanoparticles come closer to the interface, they are anchored to the interface and follow the interfacial motions.

Figure 4e shows the top view of the trajectory of the center of mass of a nanoparticle in the *xy*-plane during the MDPD simulation. Here, a high initial concentration of polymer (100 polymer strands with bending stiffness of k_b = 5 in the simulation box of 10 × 10 × 10) was used. The trajectory in Figure 4e was color-coded from red to blue, corresponding to t = 1 and 1000. Figure 4f illustrates the MSD of the center of mass of the nanoparticle during the phase separation and formation of the polymer-rich phase, averaged over 10 MDPD simulations. In Figure 4e−h, length, time, and energy scales are in MDPD units (Table S1). Figure S11 represents the MSD of the center of mass of the nanoparticle in MDPD simulations at high concentration with different bending stiffnesses of the polymer. The top view of the trajectory of the nanoparticle in a very low polymer concentration (10 polymer strands in the simulation box of 10 × 10 × 10), representing Ag-PVP-poor phase, is shown in Figure 4g. The corresponding MSD $\sim t^{0.85}$ averaged over 10 simulations (Figure 4h) suggests a subdiffusive dynamics for the nanoparticle, highlighted by the gray shaded area. These simulation results indicate that in a phase-separated medium induced by a high concentration of polymers, the nanoparticle goes through an initial super-diffusive dynamics, highlighted by the pink shaded area, regardless of the polymer bending stiffness (Figure 4f and Figure S11). Considering a power-law form for the dynamics of the nanoparticle in the superdiffusive regime, MSD $\sim t^{\alpha}$, we notice that α = 1.1, 1.3, and 1.4, corresponding to k_b = 1, 5, and 25, respectively, depicted in Figure S11. Furthermore, the transition point from the initial superdiffusive to the ultimate subdiffusive regime seems to be inversely correlated with the polymer bending rigidity, k_b. This means that for very stiff polymers like rigid rods, the nanoparticle dynamics quickly shifts from super- to subdiffusive dynamics.

Overall, the simulation results in Figures 1 and 4 suggest that the dynamics of the nanoparticle is strongly correlated with the relaxation of polymers in the polymer-rich phase. We conjecture that during the initial stages, before reaching the equilibrium configuration of polymers, the relaxation of polymers affects the dynamics of the nanoparticle at the interface of the polymer-poor and -rich phases. Relaxation of these polymers makes the nanoparticle move faster than a normal diffusion. On the other hand, after polymer relaxation and reaching an equilibrium, our simulation results indicate that the interfacial attraction restricts the motion of the nanoparticle, manifested in a subdiffusion dynamics for the nanoparticle. If the interfacial adhesion increases greatly, it can stall the motion of the nanoparticle eventually.

CONCLUSIONS

We investigate the nucleation and growth mechanism of nanoparticles in a phase-separated medium by the LPTEM. This study demonstrates that the interface plays an important role in the formation and diffusion of nanoparticles. The direct observation from this study will help understand the synthesis of nanoparticles from a nonuniform solution, which is widely used to form various metals, metal oxide nanoparticles, and nanocomposites. Our observations can also aid in understanding the complex crystallization processes from multicomponent systems.

ASSOCIATED CONTENT

Supporting Information

The Supporting Information is available free of charge at https://pubs.acs.org/doi/10.1021/acsami.1c20824.

Computational methods for the theoretical model, schematic illustration of preparing liquid cells for in situ TEM study, schematic illustration of inspecting liquid cell fabrication processes, individual trajectories and MSD plots of Ag nanoparticles, control experiment results of TEM imaging of PVP ethylene glycol solution, original TEM images of Figure 2,4, and MSD of a nanoparticle as a function of MDPD time (PDF)

Original in situ liquid phase TEM movie (MP4)

AUTHOR INFORMATION

Corresponding Authors

Taeghwan Hyeon − *Center for Nanoparticle Research, Institute for Basic Science (IBS), Seoul 08826, Republic of Korea; School of Chemical and Biological Engineering, and Institute of Chemical Process, Seoul National University, Seoul 08826, Republic of Korea;* orcid.org/0000-0001-5959-6257; Email: thyeon@snu.ac.kr

Shafigh Mehraeen − *Department of Chemical Engineering, University of Illinois at Chicago, Chicago, Illinois 60607, United States;* orcid.org/0000-0002-0066-7396; Email: tranzabi@uic.edu

Jungwon Park − *Center for Nanoparticle Research, Institute for Basic Science (IBS), Seoul 08826, Republic of Korea; School of Chemical and Biological Engineering, and Institute of Chemical Process and Institute of Engineering Research, College of Engineering, Seoul National University, Seoul 08826, Republic of Korea; Advanced Institutes of Convergence Technology, Seoul National University, Gyeonggi-do 16229, Republic of Korea;* orcid.org/0000-0003-2927-4331; Email: jungwonpark@snu.ac.kr

Authors

Youngju Son − *Center for Nanoparticle Research, Institute for Basic Science (IBS), Seoul 08826, Republic of Korea; School of Chemical and Biological Engineering, and Institute of Chemical Process, Seoul National University, Seoul 08826, Republic of Korea*

Byung Hyo Kim − *Center for Nanoparticle Research, Institute for Basic Science (IBS), Seoul 08826, Republic of Korea; Department of Organic Materials and Fiber Engineering, Soongsil University, Seoul 06978, Republic of Korea;* orcid.org/0000-0002-4098-0053

https://doi.org/10.1021/acsami.1c20824
ACS Appl. Mater. Interfaces XXXX, XXX, XXX−XXX

Back Kyu Choi − *Center for Nanoparticle Research, Institute for Basic Science (IBS), Seoul 08826, Republic of Korea; School of Chemical and Biological Engineering, and Institute of Chemical Process, Seoul National University, Seoul 08826, Republic of Korea;* orcid.org/0000-0001-8828-2660
Zhen Luo − *Department of Chemical Engineering, University of Illinois at Chicago, Chicago, Illinois 60607, United States*
Joodeok Kim − *Center for Nanoparticle Research, Institute for Basic Science (IBS), Seoul 08826, Republic of Korea; School of Chemical and Biological Engineering, and Institute of Chemical Process, Seoul National University, Seoul 08826, Republic of Korea*
Ga-Hyun Kim − *Department of Chemistry and Nanoscience, Ewha Womans University, Seoul 03760, Republic of Korea*
So-Jung Park − *Department of Chemistry and Nanoscience, Ewha Womans University, Seoul 03760, Republic of Korea;* orcid.org/0000-0002-6364-3754

Complete contact information is available at: https://pubs.acs.org/10.1021/acsami.1c20824

Author Contributions

†Y.S., B.H.K., and B.K.C. contributed equally to this work. Y.S., B.H.K, and B.K.C. wrote the manuscript. Y.S. performed and analyzed the LPTEM experiment. B.H.K. conducted the mechanistic study. Z.L. and S.M. conducted MDPD simulations. J.K. carried out binarization processing of the LPTEM images. G.K, S.P., and T.H. contributed to the discussion. J.P. wrote the manuscript and supervised the research.

Notes

The authors declare no competing financial interest.

■ ACKNOWLEDGMENTS

This research was supported by IBS-R006-D1. S.-J.P. and J.P. acknowledge the National Research Foundation of Korea (NRF) grant funded by the Korea government (MSIT) (NRF-2017R1A5A1015365). J.P. acknowledges the National Research Foundation of Korea (NRF) grant funded by the Korea government (MSIT) (NRF-2020R1A2C2101871). J.P. acknowledges support by Samsung Science and Technology Foundation under project number SSTF-BA1802-08 for the in situ TEM analysis. B.H.K. acknowledge the National Research Foundation of Korea (NRF) grant funded by the Korea government (MSIT) (NRF-2021R1C1C11014339). Z.L. and S.M. acknowledge the seed funding from the college of engineering at the University of Illinois at Chicago.

■ REFERENCES

(1) Chiu, Y. P.; Sun, Y. C.; Qiu, D. C.; Lin, Y. H.; Chen, Y. Q.; Kuo, J. C.; Huang, J. R. Liquid-liquid Phase Separation and Extracellular Multivalent Interactions in the Tale of Galectin-3. *Nat. Commun.* **2020**, *11*, 1229.
(2) Kong, D.; Nguyen, K. D. Q.; Megone, W.; Peng, L.; Gautrot, J. E. The Culture of HaCaT Cells on Lquid Substrates is Mediated by a Mechanically Strong Liquid-liquid Interface. *Faraday Discuss.* **2017**, *204*, 367−381.
(3) Piradashvili, K.; Alexandrino, E. M.; Wurm, F. R.; Landfester, K. Reactions and Polymerizations at the Liquid-Liquid Interface. *Chem. Rev.* **2016**, *116*, 2141−2169.
(4) Binks, B. P. Colloidal Particles at a Range of Fluid-Fluid Interfaces. *Langmuir* **2017**, *33*, 6947−6963.
(5) Rautaray, D.; Kavathekar, R.; Sastry, M. Using the Dynamic, Expanding Liquid-liquid Interface in a Hele-Shaw Cell in Crystal Growth and Nanoparticle Assembly. *Faraday Discuss.* **2005**, *129*, 205−217.
(6) Hashimoto, T.; Maruoka, K. Recent Development and Application of Chiral Phase-Transfer Catalysts. *Chem. Rev.* **2007**, *107*, 5656−5682.
(7) Brust, M.; Walker, M.; Bethell, D.; Schiffrin, D. J.; Whyman, R. Synthesis of Thiol-Derivatized Gold Nanoparticles in a 2-Phase Liquid-Liquid System. *J. Chem. Soc., Chem. Comm.* **1994**, *7*, 801−802.
(8) Lee, J.; Yang, J.; Kwon, S. G.; Hyeon, T. Nonclassical Nucleation and Growth of Inorganic Nanoparticles. *Nat. Rev. Mater.* **2016**, *1*, 16034.
(9) Pileni, M. P. Nanosized Particles Made in Colloidal Assemblies. *Langmuir* **1997**, *13*, 3266−3276.
(10) Wei, Z. Y.; Matsui, H. Rational Strategy for Shaped Nanomaterial Synthesis in Reverse Micelle Reactors. *Nat. Commun.* **2014**, *5*, 3870.
(11) Lee, M. W.; Kwon, D. J.; Park, J.; Pyun, J. C.; Kim, Y. J.; Ahn, H. S. Electropolymerization in a Confined Nanospace: Synthesis of PEDOT Nanoparticles in Emulsion Droplet Reactors. *Chem. Commun.* **2020**, *56*, 9624−9627.
(12) Anton, N.; Benoit, J. P.; Saulnier, P. Design and Production of Nanoparticles Formulated from Nano-emulsion Templates - A Review. *J. Controlled Release* **2008**, *128*, 185−199.
(13) Baek, J.; Shen, Y.; Lignos, I.; Bawendi, M. G.; Jensen, K. F. Multistage Microfluidic Platform for the Continuous Synthesis of III-V Core/Shell Quantum Dots. *Angew. Chem., Int. Ed.* **2018**, *57*, 10915−10918.
(14) Silvestri, A.; Lay, L.; Psaro, R.; Polito, L.; Evangelisti, C. Fluidic Manufacture of Star-Shaped Gold Nanoparticles. *Chem. Eur. J.* **2017**, *23*, 9732−9735.
(15) Bera, S.; Pradhan, N. Perovskite Nanocrystal Heterostructures: Synthesis, Optical Properties, and Applications. *ACS Energy Lett.* **2020**, *5*, 2858−2872.
(16) Baryiames, C. P.; Baiz, C. R. Slow Oil, Slow Water: Long-Range Dynamic Coupling across a Liquid-Liquid Interface. *J. Am. Chem. Soc.* **2020**, *142*, 8063−8067.
(17) Singh, P. C.; Inoue, K.; Nihonyanagi, S.; Yamaguchi, S.; Tahara, T. Femtosecond Hydrogen Bond Dynamics of Bulk-like and Bound Water at Positively and Negatively Charged Lipid Interfaces Revealed by 2D HD-VSFG Spectroscopy. *Angew. Chem., Int. Ed.* **2016**, *55*, 10621−10625.
(18) Eisenthal, K. B. Liquid Interfaces. *Acc. Chem. Res.* **1993**, *26*, 636−643.
(19) Goswami, T.; Kumar, S. K. K.; Dutta, A.; Goswami, D. Probing the Ultrafast Solution Dynamics of a Cyanine Dye in an Organic Solvent Interfaced with Water. *J. Phys. Chem. B* **2009**, *113*, 16332−16336.
(20) Fedoseeva, M.; Letrun, R.; Vauthey, E. Excited-State Dynamics of Rhodamine 6G in Aqueous Solution and at the Dodecane/Water Interface. *J. Phys. Chem. B* **2014**, *118*, 5184−5193.
(21) Yang, J.; Zeng, Z.; Kang, J.; Betzler, S.; Czarnik, C.; Zhang, X.; Ophus, C.; Yu, C.; Bustillo, K.; Pan, M.; Qiu, J.; Wang, L.-W.; Zheng, H. Formation of Two-dimensional Transition Metal Oxide Nanosheets with Nanoparticles as Intermediates. *Nat. Mater.* **2019**, *18*, 970−976.
(22) Kim, B. H.; Yang, J.; Lee, D.; Choi, B. K.; Hyeon, T.; Park, J. Liquid-Phase Transmission Electron Microscopy for Studying Colloidal Inorganic Nanoparticles. *Adv. Mater.* **2018**, *30*, 1703316.
(23) Kim, J.; Ou, Z.; Jones, M. R.; Song, X. H.; Chen, Q. Imaging the Polymerization of Multivalent Nanoparticles in Solution. *Nat. Commun.* **2017**, *8*, 761.
(24) Sung, J.; Choi, B. K.; Kim, B.; Kim, B. H.; Kim, J.; Lee, D.; Kim, S.; Kang, K.; Hyeon, T.; Park, J. Redox-Sensitive Facet Dependency in Etching of Ceria Nanocrystals Directly Observed by Liquid Cell TEM. *J. Am. Chem. Soc.* **2019**, *141*, 18395−18399.
(25) Chen, L.; Leonardi, A.; Chen, J.; Cao, M. H.; Li, N.; Su, D.; Zhang, Q.; Engel, M.; Ye, X. C. Imaging the Kinetics of Anisotropic Dissolution of Bimetallic Core-shell Nanocubes Using Graphene Liquid Cells. *Nat. Commun.* **2020**, *11*, 3041.
(26) Yang, J.; Koo, J.; Kim, S.; Jeon, S.; Choi, B. K.; Kwon, S.; Kim, J.; Kim, B. H.; Lee, W. C.; Lee, W. B.; Lee, H.; Hyeon, T.; Ercius, P.;

Park, J. Amorphous-Phase-Mediated Crystallization of Ni Nanocrystals Revealed by High-Resolution Liquid-Phase Electron Microscopy. *J. Am. Chem. Soc.* **2019**, *141*, 763−768.
(27) Kim, S.; Jung, H. J.; Kim, J. C.; Lee, K. S.; Park, S. S.; Dravid, V. P.; He, K.; Jeong, H. Y. In Situ Observation of Resistive Switching in an Asymmetric Graphene Oxide Bilayer Structure. *ACS Nano* **2018**, *12*, 7335−7342.
(28) Bae, Y.; Lim, K.; Kim, S.; Kang, D.; Kim, B. H.; Kim, J.; Kang, S.; Jeon, S.; Cho, J.; Lee, W. B.; Lee, W. C.; Park, J. Ligand-Dependent Coalescence Behaviors of Gold Nanoparticles Studied by Multichamber Graphene Liquid Cell Transmission Electron Microscopy. *Nano Lett.* **2020**, *20*, 8704−8710.
(29) Loh, N. D.; Sen, S.; Bosman, M.; Tan, S. F.; Zhong, J.; Nijhuis, C. A.; Kral, P.; Matsudaira, P.; Mirsaidov, U. Multistep Nucleation of Nanocrystals in Aqueous Solution. *Nat. Chem.* **2017**, *9*, 77−82.
(30) Liu, X. W.; Chee, S. W.; Raj, S.; Sawczyk, M.; Kral, P.; Mirsaidov, U. Three-step Nucleation of Metal-organic Framework Nanocrystals. *P. Natl. Acad. Sci. U.S.A.* **2021**, *118*, No. e2008880118.
(31) Ianiro, A.; Wu, H. L.; van Rijt, M. M. J.; Vena, M. P.; Keizer, A. D. A.; Esteves, A. C. C.; Tuinier, R.; Friedrich, H.; Sommerdijk, N. A. J. M.; Patterson, J. P. Liquid-liquid Phase Separation during Amphiphilic Self-assembly. *Nat. Chem.* **2019**, *11*, 320−328.
(32) Sen, M.; Guven, O. Determination of Solubility Parameter of Poly(n-vinyl 2-pyrrolidon/ethylene glycol dimethacrylate) Gels by Swelling Measurements. *J. Polym. Sci., Polym. Phys.* **1998**, *36*, 213−219.
(33) Barton, A. F. M. *Handbook of Solubility Parameters and Other Cohesion Parameters*; CRC Press: Boca Raton, FL, 1991; pp 291−293.
(34) Chen, Z. F.; Chang, J. W.; Balasanthiran, C.; Milner, S. T.; Rioux, R. M. Anisotropic Growth of Silver Nanoparticles Is Kinetically Controlled by Polyvinylpyrrolidone Binding. *J. Am. Chem. Soc.* **2019**, *141*, 4328−4337.
(35) Gao, Y.; Jiang, P.; Liu, D. F.; Yuan, H. J.; Yan, X. Q.; Zhou, Z. P.; Wang, J. X.; Song, L.; Liu, L. F.; Zhou, W. Y.; Wang, G.; Wang, C. Y.; Xie, S. S.; Zhang, J. M.; Shen, A. Y. Evidence for the Monolayer Assembly of Poly(vinylpyrrolidone) on the Surfaces of Silver Nanowires. *J. Phys. Chem. B* **2004**, *108*, 12877−12881.
(36) Huang, H. H.; Ni, X. P.; Loy, G. L.; Chew, C. H.; Tan, K. L.; Loh, F. C.; Deng, J. F.; Xu, G. Q. Photochemical Formation of Silver Nanoparticles in Poly(N-vinylpyrrolidone). *Langmuir* **1996**, *12*, 909−912.
(37) Pagonabarraga, I.; Frenkel, D. Dissipative Particle Dynamics for Interacting Systems. *J. Chem. Phys.* **2001**, *115*, 5015−5026.
(38) Warren, P. B. Hydrodynamic Bubble Coarsening in Off-critical Vapor-liquid Phase Separation. *Phys. Rev. Lett.* **2001**, *87*, 225702.
(39) Warren, P. B. Vapor-liquid Coexistence in Many-body Dissipative Particle Dynamics. *Phys. Rev. E* **2003**, *68*, 066702.
(40) Chen, C.; Gao, C. N.; Zhuang, L.; Li, X. F.; Wu, P. C.; Dong, J. F.; Lu, J. T. A Many-Body Dissipative Particle Dynamics Study of Spontaneous Capillary Imbibition and Drainage. *Langmuir* **2010**, *26*, 9533−9538.
(41) Chen, C.; Zhuang, L.; Li, X. F.; Dong, J. F.; Lu, J. T. A Many-Body Dissipative Particle Dynamics Study of Forced Water-Oil Displacement in Capillary. *Langmuir* **2012**, *28*, 1330−1336.
(42) Wiley, B.; Herricks, T.; Sun, Y. G.; Xia, Y. N. Polyol Synthesis of Silver Nanoparticles: Use of Chloride and Oxygen to Promote the Formation of Single-crystal, Truncated Cubes and Tetrahedrons. *Nano Lett.* **2004**, *4*, 1733−1739.
(43) Senapati, S.; Berkowitz, M. L. Computer Simulation Study of the Interface Width of the Liquid/liquid Interface. *Phys. Rev. Lett.* **2001**, *87*, 176101.
(44) Metzler, R.; Klafter, J. The Random Walk's Guide to Anomalous Diffusion: a Fractional Dynamics Approach. *Phys. Rep.* **2000**, *339*, 1−77.
(45) Sokolov, I. M. Models of Anomalous Diffusion in Crowded Environments. *Soft Matter* **2012**, *8*, 9043−9052.
(46) Zheng, H. M.; Claridge, S. A.; Minor, A. M.; Alivisatos, A. P.; Dahmen, U. Nanocrystal Diffusion in a Liquid Thin Film Observed by in Situ Transmission Electron Microscopy. *Nano Lett.* **2009**, *9*, 2460−2465.
(47) Lu, J. Y.; Aabdin, Z.; Loh, N. D.; Bhattacharya, D.; Mirsaidov, U. Nanoparticle Dynamics in a Nanodroplet. *Nano Lett.* **2014**, *14*, 2111−2115.
(48) Woehl, T. J.; Prozorov, T. The Mechanisms for Nanoparticle Surface Diffusion and Chain Self-Assembly Determined from Real-Time Nanoscale Kinetics in Liquid. *J. Phys. Chem. C* **2015**, *119*, 21261−21269.

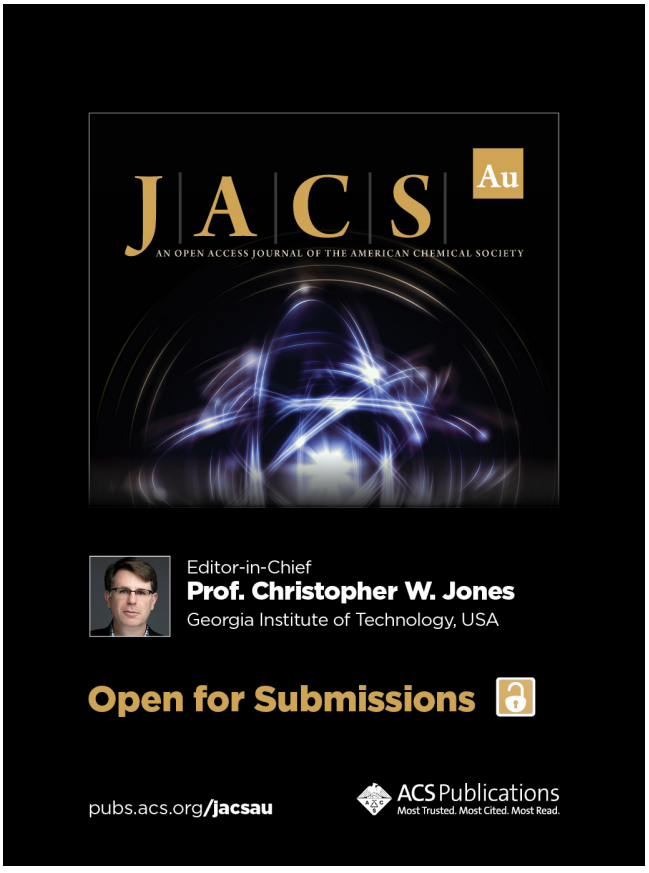

https://doi.org/10.1021/acsami.1c20824
ACS Appl. Mater. Interfaces XXXX, XXX, XXX−XXX